Available online at www.sciencedirect.com

ScienceDirect

Ceramics International 40 (2014) 4095–4107

CERAMICS INTERNATIONAL

www.elsevier.com/locate/ceramint

Effect of the fluoride content on the bioactivity of calcium silicate-based endodontic cements

Paola Taddei[a,*], Enrico Modena[a], Anna Tinti[a], Francesco Siboni[b], Carlo Prati[b], Maria Giovanna Gandolfi[b]

[a]Department of Biomedical and Neuromotor Sciences, Biochemistry Unit, University of Bologna, Via Belmeloro 8/2, 40126 Bologna, Italy
[b]Department of Biomedical and Neuromotor Sciences, Laboratory of Biomaterials and Oral Pathology, Odontostomatological Sciences Unit, University of Bologna, Via San Vitale 59, 40136 Bologna, Italy

Received 7 August 2013; accepted 14 August 2013
Available online 22 August 2013

Abstract

This study was aimed at investigating the effect of the fluoride content (added as NaF) on the *in vitro* bioactivity of an experimental calcium silicate-based cement (wTC-Bi) obtained from white Portland cement. To this purpose, wTC-Bi and fluoride-doped wTC-Bi cements (i.e. FTC-Bi and F10TC-Bi with fluoride contents of 1% and 10% w/w, respectively) were aged in Dulbecco's Phosphate Buffered Saline (DPBS) and were comparatively analysed by micro-Raman and IR spectroscopy to investigate the presence of deposits on the surface of the cements and the composition changes of the cement as a function of the storage time. Commercial White ProRoot MTA was analyzed as reference.

All the tested cements showed the formation of a calcium phosphate deposit already after 5 h of soaking. Fluoride-doped cements demonstrated a higher bioactivity than the undoped wTC-Bi cement. This result was explained in relation to the different solubility of the deposit formed on the cements: a B-type carbonated apatite on the undoped cements and a less soluble fluoride containing B-type carbonated apatite on the fluoride-doped cements. The NaF content was found to influence the apatite forming ability; actually, the cement richer in NaF, i.e. F10TC-Bi showed a lower bioactivity than FTC-Bi, which contained only 1% w/w of NaF. This result may be explained in relation to the lower hydration rate of the former, which showed the formation of lower amounts of CSH, ettringite and portlandite phases.

Keywords: B. Chemical properties; B. Spectroscopy; D. Apatite; D. Silicate; E. Biomedical applications

1. Introduction

Portland cements are hydraulic materials manufactured by roasting at about 1400 °C clay and limestone. White Portland cements are mainly composed of tricalcium silicate (alite, $3CaO \cdot SiO_2$), dicalcium silicate (belite, $2CaO \cdot SiO_2$) and minor amounts of tricalcium aluminate ($3CaO \cdot Al_2O_3$). Calcium sulphates are generally added to Portland cements to adjust the setting time, i.e. to avoid a rapid desiccation of the paste and the brittleness of the cement: a too fast setting time impedes an effective and complete hydration of the calcium silicate particles of the cement.

In the last two decades, calcium silicate-based cements have received an increasing consideration in endodontics because they are hydraulic cements that set in the presence of water and biological fluids, an important property for dental cements. Therefore, in the 1990s, a new material, MTA (mineral trioxide aggregate) was developed as root-end filling material. As reported by the patent [1], MTA is a type I ordinary Portland cement with a 4:1 addition of bismuth oxide (radiopacifier).

It is well established that the hydration of MTA-based cements involves a number of chemical reactions that take place simultaneously. The hydrolysis of calcium silicates produces a nanoporous gel of calcium silicate hydrates (CSH phase) and calcium hydroxide (portlandite). The presence of the latter makes the hydrated cement highly alkaline [2] and leads to a calcium release in the surrounding environment. From the reaction between tricalcium aluminate and gypsum with water, ettringite ($3CaO \cdot Al_2O_3 \cdot 3CaSO_4 \cdot 32H_2O$) is also produced.

*Corresponding author. Tel./fax: +39 051 209 4280.
E-mail address: paola.taddei@unibo.it (P. Taddei).

0272-8842/$ - see front matter © 2013 Elsevier Ltd and Techna Group S.r.l. All rights reserved.
http://dx.doi.org/10.1016/j.ceramint.2013.08.064

MTAs and calcium silicate-based cements appear very promising materials due to their well-documented bioactivity [3–9]. According to the European Society for Biomaterials (ESB) Consensus Conference of 1987 [10], a bioactive material must be able "to induce specific biological activity". This definition has been subsequently refined so that, according to Kokubo and Takadama [11], bioactive materials are considered as bone bonding materials, i.e. as materials that form bone-like apatite upon immersion in a serum-like solution. In other words, they are able to accelerate heterogeneous apatite crystallization in a solution supersaturated towards hydroxyapatite [11]. Actually, the deposition of hydroxyapatite-like calcium phosphates on the biomaterial surface may facilitate the direct bonding to bone and represents an essential requirement for osteoconduction and osteoinduction [12]. Moreover, bioactive calcium silicate cements may induce remineralisation of partially demineralised dentine [13,14].

Although false positive and false negative results can be occasionally obtained [15], the use of abiotic calcifying media that simulate body fluids in inorganic ion concentrations (i.e. simulated body fluids, SBFs) is a currently accepted method to study the mechanism of biomaterials calcification. The study of the bioactivity *in vitro* is useful to predict the apatite formation ability *in vivo*.

Fluoride plays an important role in tissue mineralization processes, supplying clinical benefits. It may remineralize enamel and softened dentine, reducing caries formation [16]; actually, fluoride ions have been traditionally incorporated into dental resins and glass ionomer cements to increase the remineralisation properties of filling materials [17]. Several studies have demonstrated the high activity of fluorine on osteoblastic cells and have reported that micromolar fluoride concentrations are effective to improve the cell attachment and the subsequent cell activities and to stimulate proliferation of osteoblast progenitor, osteoblast and osteoblast-like cells [18,19], improving mineralization and bone formation *in vivo* [20].

With regards to calcium silicate cements, Gandolfi et al. reported that the addition of fluoride (1% w/w) causes an increase in expansion, setting time [21], long-term apical sealing ability [22], and an improvement of the biological behavior [23].

In this context, our study was aimed at investigating the effect of the fluoride content on the in vitro bioactivity of an experimental calcium silicate-based cement (wTC-Bi) obtained from white Portland cement. To this purpose, wTC-Bi and fluoride-doped wTC-Bi cements (with fluoride contents of 1% and 10% w/w) were aged in a SBF solution, i.e. Dulbecco′s Phosphate Buffered Saline (DPBS) and were comparatively analysed by micro-Raman and IR spectroscopy to investigate the presence of deposits on the surface of the cements and the composition changes of the cement as a function of the storage time. Commercial White ProRoot MTA was analyzed as reference. Since this cement contains bismuth oxide as radiopacifer, also the experimental cements were added with this component.

2. Materials and methods

2.1. Cements preparation and ageing experiments

To prepare the experimental wTC-Bi, FTC-Bi and F10TC-Bi, the Portland cement powder (CEM I white Aalborg, Aalborg, Denmark) was thermally and mechanically treated, added with 5% w/w calcium chloride and 17% w/w bismuth oxide. Sodium fluoride 1% w/w or 10% w/w was added to wTC-Bi to produce two experimental fluoride-doped cements, identified as FTC-Bi and F10TC-Bi, respectively.

The cement powder was mixed with DPBS (Cambrex Bio Science Verviers s.p.r.l., Belgium, cat. n.BE17-512) for 15 s (powder/liquid ratio 3:1 w/w), then layered on a plastic coverslip (Thermanox, diameter 1.2 cm) to obtain standard disks. Mechanical vibrations were used to make the disk surfaces flat and regular, with a $1.1 \pm 0.1\ cm^2$ exposed surface area.

White ProRoot MTA (Dentsply, Tulsa, OK, USA) disks were prepared analogously by mixing for 30 s on a glass slab the calcium-silicate mineral powder with the provided liquid, i.e. deionized water, following the manufacturer directions.

After preparation, the disks were immediately immersed in 5 mL of DPBS (15 mL of medium for 1 g of cement paste) and maintained at 37 °C. The samples were soaked in DPBS for different times (i.e. 5 hours, 1 day, 7, 14 and 28 days). DPBS is a physiological-like buffered (pH 7.4) Ca- and Mg-free solution composed of (mmol L^{-1}): K^+ (4.18), Na^+ (152.9), Cl^- (139.5) and PO_4^{3-} (9.56, sum of $H_2PO_4^-$ (1.5) and HPO_4^{2-} (8.06)). The storage media were renewed every week.

2.2. Spectroscopic measurements

Micro-Raman spectra were recorded in situ on the samples maintained in their storage media, to prevent any transformation. The spectra were obtained using an argon laser (Innova Coherent 70; Coherent Inc., Santa Clara, CA, USA) operating at 514 nm and a Jasco NRS-2000C micro-Raman spectrometer (Jasco Inc., Easton, MD, USA) equipped with a 160 K frozen digital CCD detector (Spec-10: 100B, Roper Scientific Inc. Trenton, NJ, USA) employing a microscope of 20 × magnification. Under these conditions, laser spot size was about 5 μm. All the spectra were recorded in back-scattering conditions with 5 cm^{-1} spectral resolution and a power on the sample of about 50 mW. The unhydrated powders of the cements were analyzed as control.

IR spectra were recorded using a Nicolet 5700 FTIR (Thermo Electron Scientific Instruments Corp., Madison, WI, USA), equipped with a Smart Orbit diamond attenuated total reflectance (ATR) accessory and a DTGS detector; the spectral resolution was 4 cm^{-1}. The ATR area had a 2 mm diameter. Under this instrumental setup, the IR radiation penetration into the cement was about 2 μm. The aged samples were analyzed after air-drying at room temperature.

To minimize problems deriving from the possible sample inhomogeneity, five Raman and IR spectra at least were recorded on each specimen area (i.e. upper surface, inner fractured

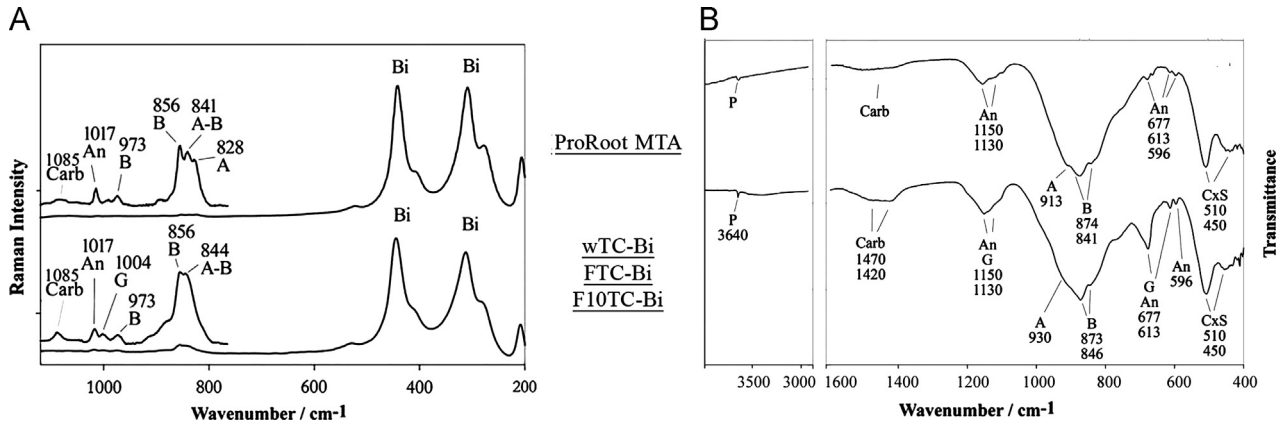

Fig. 1. Micro-Raman (A) and ATR-FTIR (B) spectra recorded on the unhydrated powders of the cements. The bands due to calcium carbonate (Carb), anhydrite (An), gypsum (G), belite (B), alite (A), poorly polymerized silicates (CxS), portlandite (P) and bismuth oxide (Bi) are indicated.

side). The deposit dispersed in the medium was filtered, dried and analyzed by IR spectroscopy. The presented spectra are representative of the obtained measurements. Intensity ratios were calculated as peak heights.

2.3. pH Measurements

The pH of the soaking solutions was measured using a Denver Instrument Basic pH meter (Denver Instruments, Bohemia, NY, USA), equipped with a Hamilton liquid-glass electrode and ± 0.01 resolution, which had previously been calibrated with acidic and neutral standard solutions. pH was measured at room temperature (24 °C) after 5 h, 1, 7, 14 and 28 days of ageing.

3. Results and discussion

3.1. Unhydrated powders

Fig. 1 shows the micro-Raman (A) and ATR/FT-IR (B) spectra recorded on the unhydrated powders of the cements. No evidence of the doping agent was observed (NaF is Raman and IR inactive), so that the spectra of wTC-Bi, FTC-Bi and F10TC-Bi were practically coincident.

The Raman spectra of wTC-Bi, FTC-Bi and F10TC-Bi (Fig. 1A) showed the presence of calcium silicates as monoclinic belite ($2CaO \cdot SiO_2$, β-polymorph) and monoclinic alite ($3CaO \cdot SiO_2$): the components at 973 cm^{-1} (ν_3 SiO_4^{4-}) and 856 cm^{-1} (ν_1 SiO_4^{4-}) are characteristic of the former [24,25], while the band at 844 cm^{-1} (ν_1 SiO_4^{4-}) can be assigned to both [25,26]. In the spectrum of ProRoot MTA, the presence of a supplementary band at 828 cm^{-1} (assignable to monoclinic alite) and the higher resolution of the silicates bands suggested a more crystalline phase of the commercial cement with respect to the experimental ones.

Calcium sulphate was present as both $CaSO_4$ (anhydrite) and $CaSO_4 \cdot 2H_2O$ (gypsum) in the unhydrated powders of wTC-Bi, FTC-Bi and F10TC-Bi as revealed by the characteristic ν_1 SO_4^{2-} bands at 1017 and 1004 cm^{-1}, respectively [27]. The absence of the latter band in the spectrum of ProRoot MTA indicates that calcium sulphate was present only as anhydrite.

The spectra of all the cements showed strong bands below 600 cm^{-1}, due to bismuth oxide, and a feature at 1085 cm^{-1} (ν_1 CO_3^{2-} symmetric stretching), assignable to calcium carbonate [28] as calcite and/or aragonite. The presence of the latter component has not been reported in the material safety data sheet (MSDS) of ProRoot MTA. Although its spectrum was recorded immediately after the opening of the package, small amounts of calcium carbonate were detected, probably due to a certain hydration in storage that leads to the formation of calcium hydroxide as portlandite (detected by IR spectroscopy, band at 3640 cm^{-1}, see Fig. 1B), which, exposed to the air, forms calcium carbonate. The Raman band at 360 cm^{-1}, characteristic of calcium hydroxide, was not detected because covered by the strong bands of bismuth oxide.

IR spectroscopy confirmed the Raman findings on cements composition. The bands due to alite and belite were observed in the IR spectra of all the starting materials: in the silicate stretching region, the higher wavenumber band (observed at 930 and 913 cm^{-1} in the experimental cements and ProRoot MTA, respectively) was assigned to the former [29], and the components at about 874 and 846 cm^{-1} were attributed to the latter [30].

The components at 450 and 510 cm^{-1}, due to the vibrational modes of poorly polymerized silicate tetrahedra (in-plane ν_2 and out-of-plane ν_4 SiO_4^{4-} bending modes, respectively [31]), were observed for all the unhydrated materials.

The weak bands at about 1420 and 1470 cm^{-1} (ν_3 CO_3^{2-} antisymmetric stretching vibration), typical of calcite and aragonite, respectively, confirmed the presence of the calcium carbonate component [32,33].

At IR spectroscopy, the most significant difference between the cements was related to calcium sulphate content. The unhydrated powder of wTC-Bi, FTC-Bi and F10TC-Bi showed the presence of both gypsum and anhydrite: the bands at 1150–1130 cm^{-1} (triply degenerate stretching mode), 677 and 613 cm^{-1} (bending

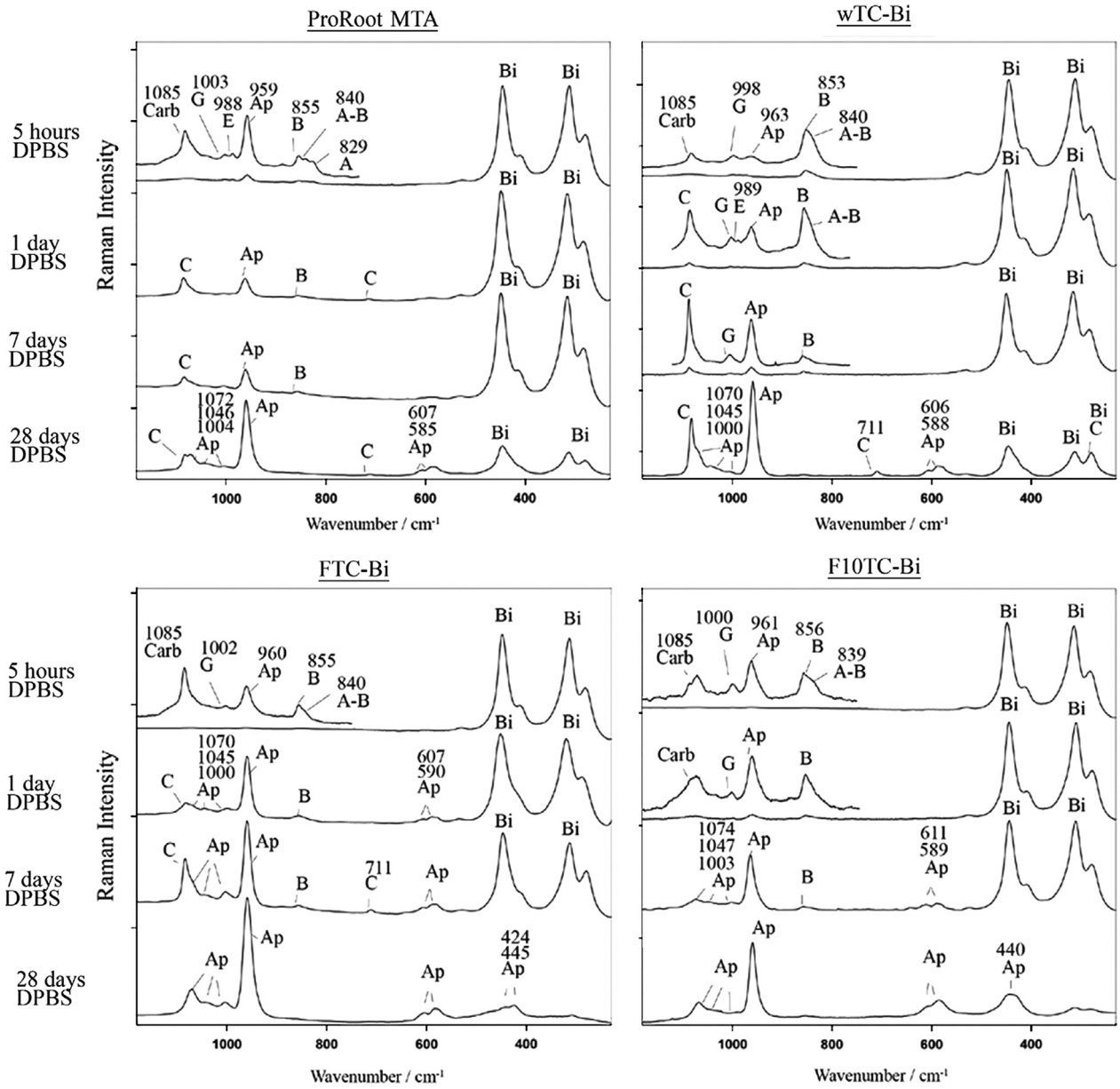

Fig. 2. Micro-Raman spectra recorded on the surface of the cements after ageing in DPBS for 5 h, 1 day, 7 and 28 days. The bands due to calcium carbonate (Carb), calcite (C), apatite (Ap), belite (B), alite (A), ettringite (E), gypsum (G) and bismuth oxide (Bi) are indicated.

modes) were common to calcium sulphates in both the anhydrite and gypsum forms, while the component at 596 cm^{-1} was characteristic of anhydrite [34]. On the basis of the relative intensities of these bands, a higher amount of calcium sulphates (as gypsum and anhydrite) in the experimental cements may be deduced; the lower content in ProRoot MTA was mainly present as anhydrite, according to Raman findings.

3.2. Ageing in DPBS

Ageing in DPBS induced significant transformations both in the cement surface and in the inner matrix.

Fig. 2 shows the Raman spectra recorded on the surface of the cements after soaking in DPBS: already after 5 h of immersion, the band at about 960 cm^{-1} (ν_1 PO_4^{3-} stretching) [35] was observed for all the cements indicating the presence of a calcium phosphate deposit. This phase forms upon combination of the calcium ions released by the cement (since DPBS is calcium-free), a well-known phenomenon [13,36], and the phosphate ions present in the ageing medium.

In the Raman spectra recorded on the surface of the cements, the spectral features assigned to the underlying cement (i.e. calcium silicates, gypsum, bismuth oxide) were still visible. The anhydrite band disappeared in all the cements, suggesting the hydration of this component to form gypsum; in the spectra of ProRoot MTA (5 h of ageing) and wTC-Bi (1 day of ageing), also the characteristic band of ettringite at 988 cm^{-1} (ν_1 SO_4^{2-} stretching) was detected [37].

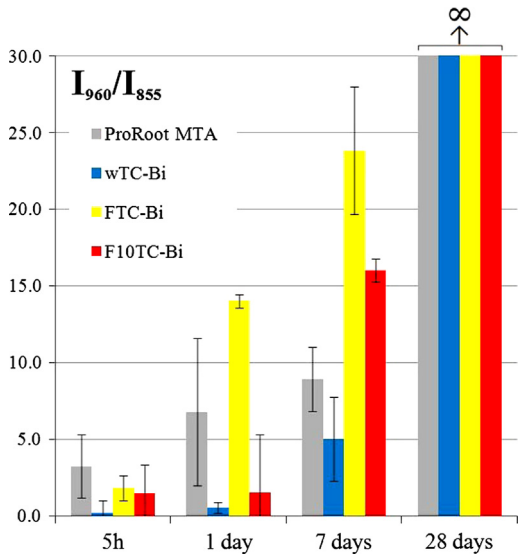

Fig. 3. $I_{960(Ap)}/I_{855(B)}$ Raman intensity ratio calculated from the spectra recorded on the surface of the cements at different times of incubation in DPBS.

At increasing ageing times, the relative intensity of the phosphate band at 960 cm^{-1} increased; after 1 day of ageing, the spectrum of FTC-Bi showed also bands at 1070 cm^{-1} (ν_1 CO_3^{2-} symmetric stretching in B-type carbonated apatites), 1045 cm^{-1} (ν_3 PO_4^{3-} antisymmetric stretching), 607–590 cm^{-1} (ν_4 PO_4^{3-} bending), ascribable to the formation of a B-type carbonated apatite deposit [35]; the band at 1000 cm^{-1} suggested the presence of HPO_4^{2-} ions in the apatite lattice [38]. The latter bands were detected after 7 days for F10TC-Bi and only after 28 days for ProRoot-MTA and wTC-Bi.

To evaluate the relative thickness of the deposits on the four cements, the $I_{960(Ap)}/I_{850(B)}$ Raman intensity ratio was calculated from the spectra recorded at different ageing times on the upper surface of the cements, and its trend is shown in Fig. 3. As can be easily seen, at times longer than 5 h, FTC-Bi exhibited the thickest deposit, while wTC-Bi the thinner one; moreover, the deposit formed on the former appeared always thicker than that on F10TC-Bi. After 28 days of soaking (Fig. 2), the 850 cm^{-1} belite band became undetectable ($I_{960(Ap)}/I_{850(B)} \rightarrow \infty$); the bands of bismuth oxide were still visible in the spectra recorded on the surface of ProRoot MTA and wTC-Bi, while became undetectable in those recorded in FTC-Bi and F10TC-Bi, making visible the PO_4^{3-} bending bands at about 440–420 cm^{-1} (ν_2 PO_4^{3-} in-plane bending [35]); these trends further suggested that the fluoride-doped cements were characterized by a more pronounced bioactivity. Calcite (revealed by the ν_4 CO_3^{2-} in-plane bending spectral feature at 711 cm^{-1}) was detected only on the surface of the wTC-Bi and ProRoot MTA cements.

Fig. 4 reports the IR spectra recorded on the upper surface of the four cements aged for different times in DPBS. The IR spectrum recorded on the FTC-Bi surface after 5 h of ageing in DPBS showed the bands due to a B-type carbonated apatite at 1462–1418 cm^{-1} (ν_3 CO_3^{2-} antisymmetric stretching in B-type carbonated apatites), 1025 cm^{-1} (ν_3 PO_4^{3-} antisymmetric stretching), 960 cm^{-1} (ν_1 PO_4^{3-} symmetric stretching), 870 cm^{-1} (ν_2 CO_3^{2-} out-of-plane bending in B-type carbonated apatites), 600–560 cm^{-1} (ν_4 PO_4^{3-} out-of-plane bending [35]); at the same time, some bands ascribable to the underlying cement or its hydration products were observed at 1110 cm^{-1} (ettringite [31]), 502 cm^{-1} (poorly polymerized silicate tetrahedral [31]), 454 cm^{-1} (CSH phase [31]). The latter result suggests that the deposit should be thinner than 2 μm, which is the average IR penetration depth using a diamond crystal in the ATR technique.

Actually, the most intense apatite band at about 1025 cm^{-1} was detected in the spectra recorded on the surface of all cements (Fig. 4), suggesting that at 5 h of ageing a calcium phosphate deposit already formed on all the materials under investigation. However, the absence of the other marker bands of B-type carbonated apatite (as in the case of ProRoot MTA), or their lower relative intensity (as in the case of wTC-Bi and F10TC-Bi) suggests that, at this stage, on ProRoot MTA, wTC-Bi and F10TC-Bi a deposit meanly thinner than on FTC-Bi formed. This result could appear in contrast with the thickness estimation made by Raman spectroscopy (see Fig. 3); actually, it must be stressed that for ATR/FT-IR spectroscopy the sampling area was significantly higher than for micro-Raman spectroscopy. Consequently, at short ageing times, when the homogeneity of the deposit may be still low, the two techniques could appear to provide not perfectly coincident results. At higher ageing times, already after one day of soaking, the bands due to the cement completely disappeared except than on wTC-Bi; actually, according to the relative value of the $I_{960(Ap)}/I_{855(B)}$ Raman intensity ratio (see Fig. 3), this cement appeared to be covered by a thinner deposit. With regards to the F-doped cements, the full width at half maximum of the IR phosphate band at about 1025 cm^{-1} ($FWHM_{1025}$, see Table 1) was always higher on F10TC-Bi than on FTC-Bi; moreover, the IR apatite band at about 960 cm^{-1} appeared less prominent than for the other cements. These trends suggest that the deposit on F10TC-Bi was characterized by a lower crystallinity.

The IR spectra confirmed the Raman results on the calcium carbonate content; at every ageing time, the deposit formed on ProRoot MTA and wTC-Bi contained calcite (bands at about 1415, 870 and 711 cm^{-1} [32]); aragonite was also revealed (bands at about 1460, 1080, 850 and 711–700 cm^{-1} [33]). At this purpose, it must be observed that the marker band at 711 cm^{-1} may be utilized to evaluate the possible presence of calcite, since its other bands were coincident with those of carbonated apatites. The lack of this band in the spectra recorded on the surface of FTC-Bi and F10TC-Bi after 28 days of ageing allowed to exclude the presence of calcite and made possible to evaluate the carbonate content of the B-type carbonated apatite formed at this stage on the two cements, by calculating the intensity ratio between the carbonate band at about 1415 cm^{-1} and the phosphate band at about 560 cm^{-1} (I_{1415}/I_{560}), according to the method described by Featherstone et al. [39]. Obviously, this evaluation is not possible in presence of calcite, due to its

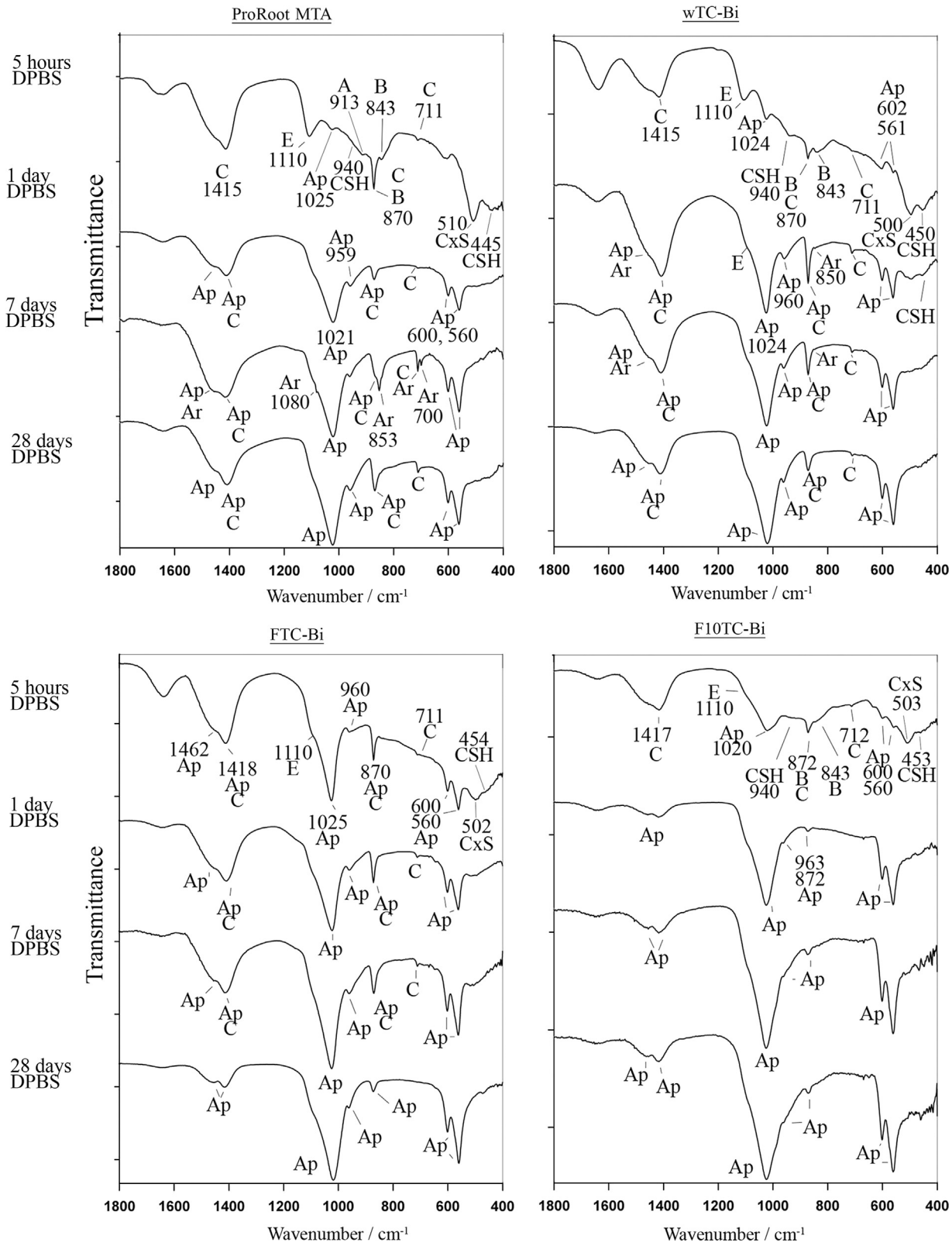

Fig. 4. IR spectra recorded on the surface of the cements after ageing in DPBS for 5 h, 1 day, 7 and 28 days. The bands due to calcite (C), aragonite (Ar), apatite (Ap), alite (A), belite (B), ettringite (E), poorly polymerized silicates (CxS) and hydrated silicate gel (CSH) are indicated.

contribution to the band at 1415 cm^{-1}. The I_{1415}/I_{560} determined from the spectra recorded on FTC-Bi and F10TC-Bi after 28 days were 0.38 and 0.30, respectively. These data suggest that the deposit formed on the former cement contained a slightly higher amount of carbonate in the carbonated apatite lattice than the latter.

Table 1
Full width at half maximum of the IR band at about 1025 cm^{-1} ($FWHM_{1025}$) as obtained from the spectra recorded on the surface of the cements and on the powders isolated from the ageing medium (into parentheses).

Time of ageing in DPBS	$FWHM_{1025}$ (cm^{-1})			
	ProRoot MTA	wTC-Bi	FTC-Bi	F10TC-Bi
1 day	93 (94)	77 (79)	84 (96)	89 (93)
7 day	92 (97)	85 (77)	84 (87)	102 (146)
28 day	88 (128)	89 (97)	90 (120)	124 (135)

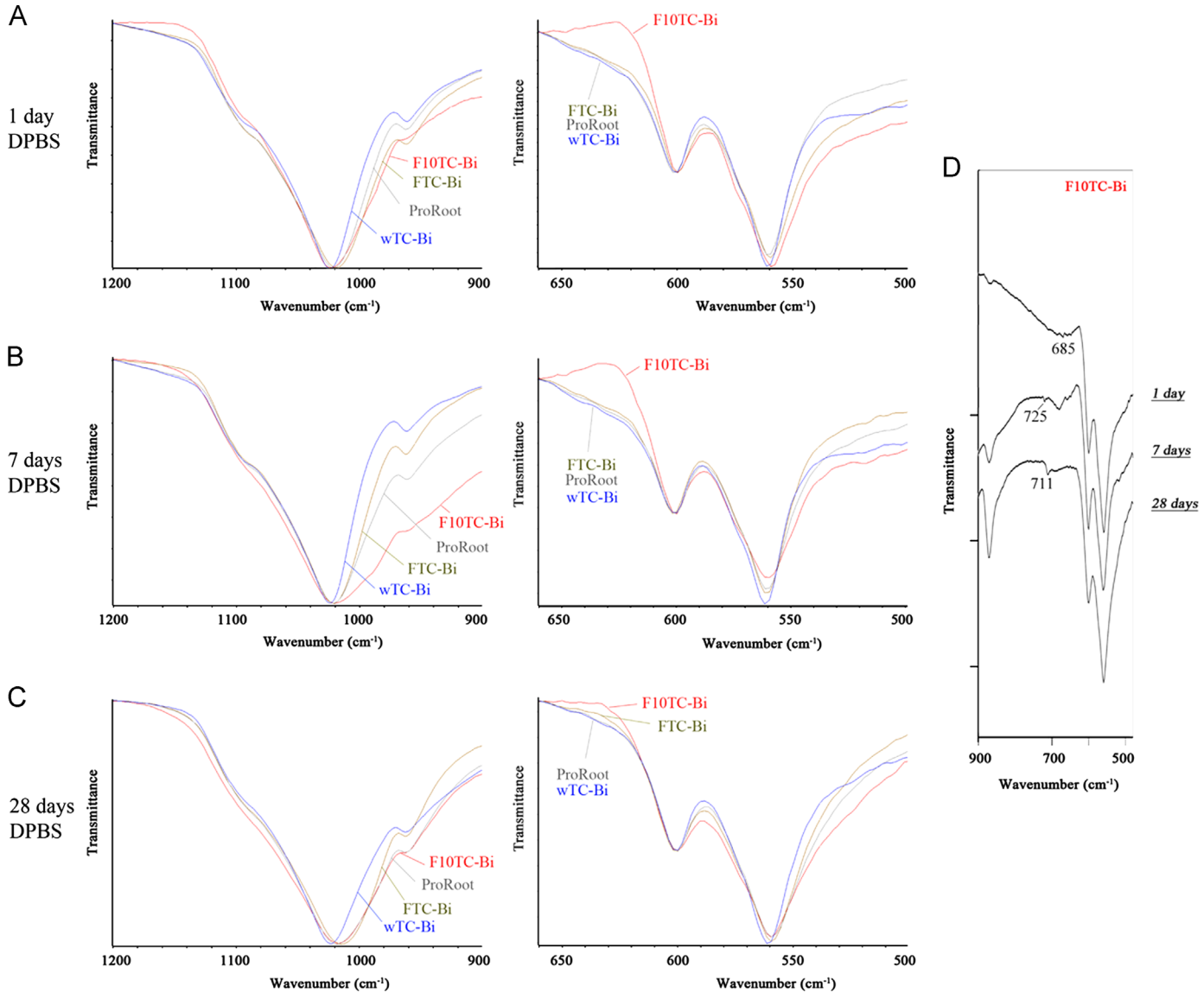

Fig. 5. IR spectra recorded on the powders isolated from the soaking media where wTC-Bi, FTC-Bi, F10TC-Bi and ProRoot MTA aged for 1 day (A), 7 days (B) and 28 days (C). (D) IR spectra recorded on the powders isolated from the soaking media where F10TC-Bi aged for 1 day, 7 and 28 days.

To gain more insight into the nature of the apatite deposit, the powder formed in the ageing medium at different soaking times was analyzed by IR spectroscopy. Fig. 5 shows the IR spectra recorded on the powders isolated from the soaking media where wTC-Bi, ProRoot-MTA, FTC-Bi and F10TC-Bi aged for 1 day, 7 and 28 days. Unfortunately, the presence of calcite (bands not shown) in most spectra makes impossible the evaluation of the carbonate content of the apatite lattice.

As reported for the spectra recorded on the surface, for F10TC-Bi the band at about 1025 cm^{-1} appeared broader (see Table 1) and the component at 960 cm^{-1} less distinct than for the other cements, confirming a less crystalline morphology of

the powder; moreover, it can be easily seen that also the bending mode at 560 cm^{-1} appeared broader. These results may be explained in relation to the trend of the band at 630 cm^{-1} (δOH bending in pure hydroxyapatite) [39,40]. Amberg et al. have analyzed by IR spectroscopy fluorinated hydroxyapatites characterized by different fluoridation degrees; these authors have observed that the intensity of the band at 630 cm^{-1} generally decreases as the extent of fluoridation increases and have interpreted this trend as a sign that fluoride exchanges to a considerable extent with either lattice hydroxyl groups or water molecules in hydroxyl sites [41]. The spectra displayed in Fig. 5A–C show that at all ageing times the shoulder at 630 cm^{-1} was markedly weaker for F10TC-Bi than for the other cements; on the basis of this trend, it may be deduced that the highest degree of fluoridation was attained by the powder formed in the presence of F10TC-Bi. After 28 days of soaking, the degree of fluoridation of the B-type carbonated apatite decreased along the series F10TC-Bi > FTC-Bi > wTC -Bi ~ ProRoot MTA (no-fluoride containing B-type carbonated apatite).

It is not surprising that the powder formed in the presence of F10TC-Bi was the least ordered, since hydroxyl replacement induces a crystal rearrangement. The region above 650 cm^{-1} allows for the evaluation of the interactions between OH^- and

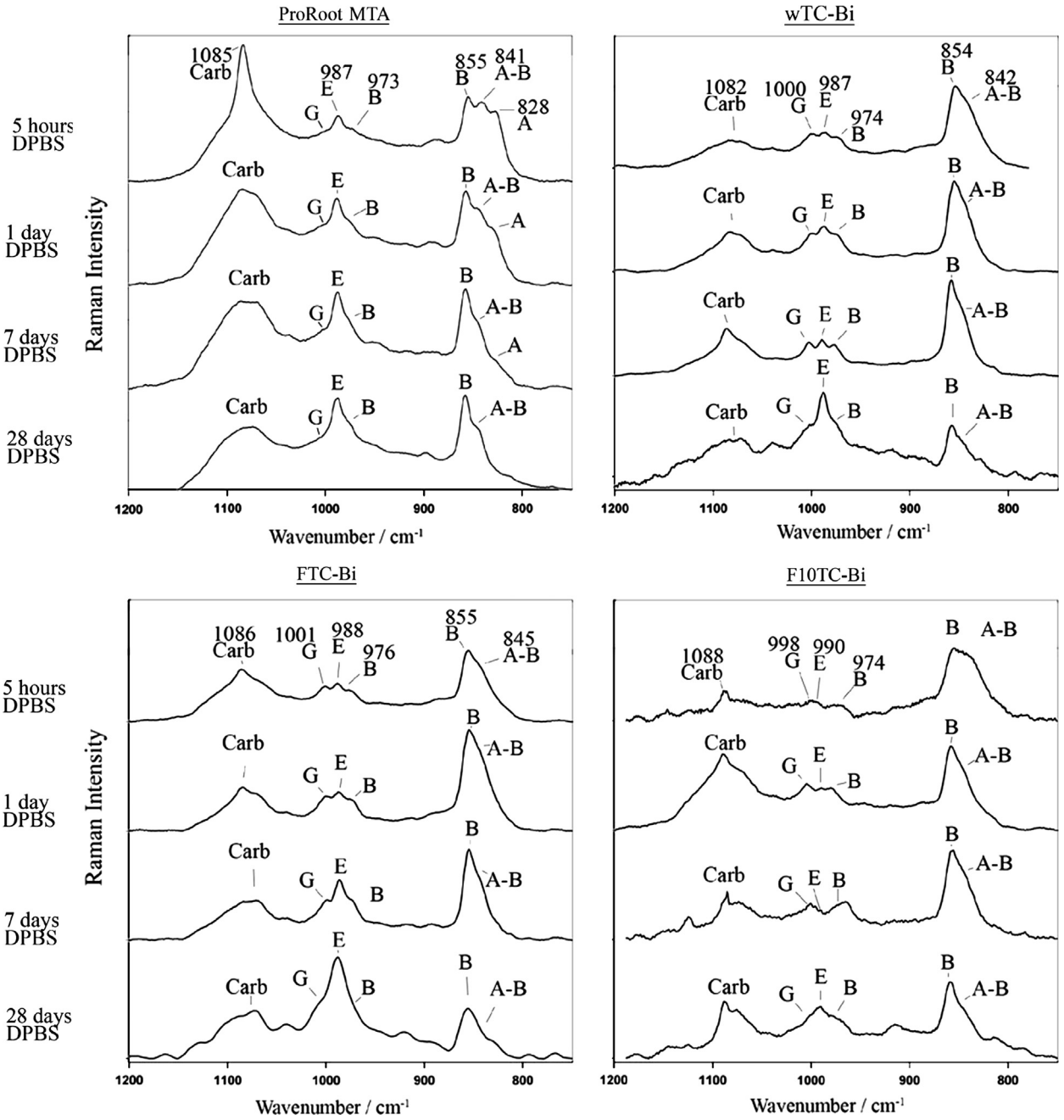

Fig. 6. Micro-Raman spectra recorded in the inner fractured section of the cements after ageing in DPBS for 5 h, 1 day, 7 and 28 days. The bands due to calcium carbonate (Carb), belite (B), alite (A), ettringite (E) and gypsum (G) are indicated.

F^- groups in fluoride containing apatites, according to the literature [42,43]. As reported by Freund and Knobel [42], on introduction of fluoride, the band at about 630 cm^{-1} shifts to higher wavenumbers and weakens, due to the occurrence of $\cdots FHO(HO)_nHO{:}OH(OH)_nOHF\cdots$ chains. Actually, the spectra reported in Fig. 5D, corresponding to the powders isolated from the medium where F10TC-Bi aged, showed a weak and broad band at about 685 cm^{-1}, which was assigned by Freund and Knobel [42] to the 'tail-to-tail' $\cdots$ HO:OH$\cdots$ configuration. In addition, the spectrum corresponding to the ageing for 7 days shows also a band at 725 cm^{-1}, assigned by Freund and Knobel [42] to an OH^- bonded to one F^-. A deeper inspection of the spectra reported in Fig. 4 allows to identify the above mentioned broadening at about 685 cm^{-1} also on the surface of F10TC-Bi.

The incorporation of fluoride into the apatite lattice gives rise to a more compact structure [44]; moreover, it is well known that fluoride substitution leads to an increase in the overall stability of hydroxyapatite in solution [45,46] and a significant decrease of the apatite solubility (K_{sp} for fluorapatite and hydroxyapatite are $6.5 \cdot 10^{-65}$ and $7.36 \cdot 10^{-60}$, respectively). Actually, among bioactive apatites, fluorinated apatites present the best in vivo chemical stability, a good integration with bone and a negligible long-term degradation [47,48]. On the other hand, solubility of carbonated fluorapatites increases with increasing CO_3^{2-} concentration in chemical and biological media [49].

The spectroscopic analyses showed that the F-doped cements were more bioactive than the other no-F containing cements; this result can be explained in relation to the lower solubility of the F-substituted apatites. However, our results would show that F10TC-Bi had a lower bioactivity than FTC-Bi; in other words, the tests performed allow to conclude that the increase in the fluoride content up to 10% w/w did not lead to an improvement in the apatite forming ability. This result is not surprising. Actually, Lin et al. [50] have evaluated the bioactivity of tricalcium silicate samples doped with 1%, 2% and 3% w/w of CaF_2 and have reported that the specimen with the highest fluoride content did not express the highest apatite forming ability. The analysis of the spectra recorded in the interior of the samples allows to gain more insights into this subject, giving information on the progress of the hydration reaction in the concrete matrix.

Fig. 6 shows the Raman spectra recorded on internal fractured section of the cement after 5 h, 1 day, 7, 14 and 28 days of ageing in DPBS. The bands characteristic of silicates (at about 975 and 855–820 cm^{-1}), calcium carbonate (at about 1085 cm^{-1}), gypsum (at about 1000 cm^{-1}) and ettringite (at about 990 cm^{-1}) were present at all ageing times. As can be easily seen by comparing the spectra recorded in the interior of the cements, the relative intensities of the bands of ettringite and belite were significantly different in the different materials. After 28 days of ageing, ProRoot MTA showed with the highest intensity the 855 cm^{-1} belite band. At all ageing times, the interior of the F10TC-Bi cement displayed the 990 cm^{-1} ettringite band with the lowest intensity. From this qualitative observation, it appears clear that the progress of the hydration process may be followed by analyzing the trend of the relative intensities of the bands at 990 and 855 cm^{-1}; the former reflects the production of ettringite upon the reaction between calcium aluminate, calcium sulphates and water, the latter the consumption of calcium silicates that undergo hydration. For a quantitative analysis, the trend of the $I_{990(E)}/I_{855(B)}$ Raman intensity ratio is reported in Fig. 7. The wTC-Bi and FTC-Bi cements showed a marked increase of the $I_{990(E)}/I_{855(B)}$ intensity ratio at long ageing times, while F10TC-Bi showed a slight increment, suggesting a slower hydration rate. FTC-Bi expressed a faster ettringite formation also with respect to the undoped wTC-Bi cement. With regards to the commercial ProRoot MTA cement, the trend of the intensity ratio suggested an intermediate behavior closer to the "slower" F10TC-Bi cement than to the "faster" wTC-Bi and FTC-Bi cements. As above reported and as visible in Fig. 6, the commercial cement was characterized by a more crystalline silicate component, which evidently hydrates more slowly.

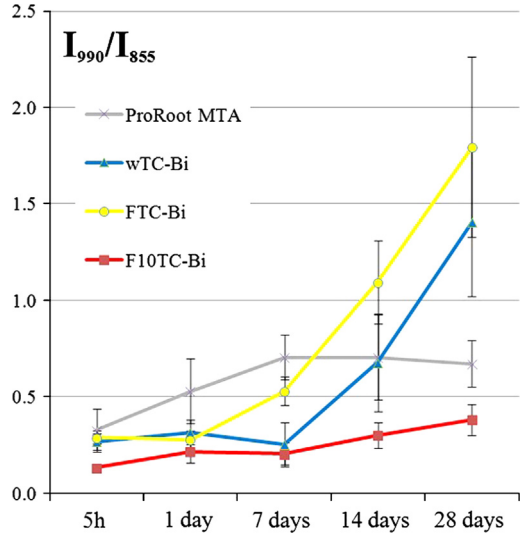

Fig. 7. Trend of the $I_{990(E)}/I_{855(B)}$ Raman intensity ratio calculated from the spectra recorded in the inner fractured section of the cements at different times of incubation in DPBS.

Fig. 8 shows the IR spectra recorded in the inner fractured section of the cements after ageing in DPBS for 5 h, 1 day, 7 and 28 days.

After 5 h of ageing, the marker bands of belite (at about 872 and 845 cm^{-1}), poorly polymerized silicates (CxS, band at about 500 cm^{-1}), ettringite (at about 1110 cm^{-1}), CSH phase (at about 930 and 450 cm^{-1}), and calcium carbonate (at about 1415, 1470 and 872 cm^{-1}) were detected in the spectra of all cements. As ageing proceeded, the band at about 450 cm^{-1}, due to the contribution of the CSH phase, increased in intensity with respect to the 500 cm^{-1} component, assigned to poorly polymerized tetrahedra; at the same time, the main CSH band above 900 cm^{-1} increased in intensity with respect to the 845 cm^{-1} belite band, and shifted to higher wavenumbers (from about 930 to 955 cm^{-1}), indicating the progress of the hydration process and the formation of the CSH phase. The IR $I_{940(CSH)}/I_{845(B)}$ intensity ratio may be a quantitative marker of

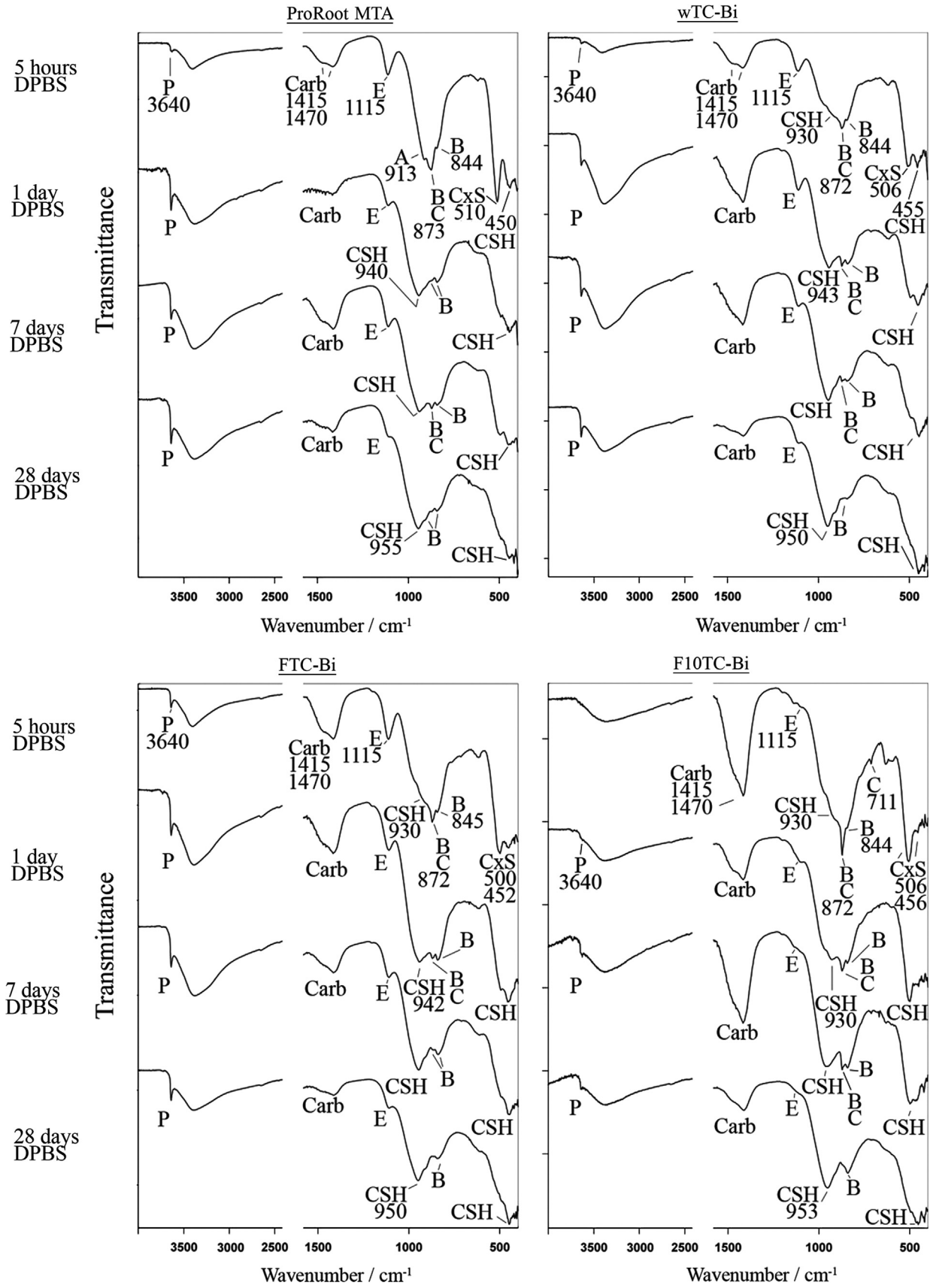

Fig. 8. IR spectra recorded in the inner fractured section of the cements after ageing in DPBS for 5 h, 1 day, 7 and 28 days. The bands prevalently due to portlandite (P), calcite (C), calcium carbonate (Carb), ettringite (E), alite (A), belite (B), hydrated silicate gel (CSH) and poorly polymerized silicate tetrahedra (CxS) are indicated.

the hydration of belite to produce the CSH phase; the F10TC-Bi cement showed the lowest value of this ratio at any ageing time, suggesting that in this material the hydration of the silicate phase was the slowest. Interestingly, after 28 days of ageing, the IR $I_{940(CSH)}/I_{845(B)}$ intensity ratio decreased along the series: FTC-Bi ($I_{940(CSH)}/I_{845(B)}=1.88$) > wTC-Bi ($I_{940(CSH)}/I_{845(B)}=1.81$) > ProRoot MTA and F10TC-Bi ($I_{940(CSH)}/I_{845(B)}=1.55$). As above stressed, the low value observed for ProRoot MTA may be related to the higher crystalline character of the silicate component.

An analogously low hydration rate may be deduced also for the calcium aluminate and sulphate phases; actually, in F10 TC-Bi, at any ageing time, the marker band of ettringite was weaker than in the other cements, confirming the Raman findings. Actually, after 28 days of ageing, the IR $I_{1110(E)}/I_{845(B)}$ ratio in the different cements had the same trend as the corresponding Raman $I_{990(E)}/I_{855(B)}$ ratio (Fig. 7); actually, the former decreased along the series: FTC-Bi ($I_{1110(E)}/I_{845(B)}=0.29$) > wTC-Bi ($I_{1110(E)}/I_{845(B)}=0.20$) > ProRoot MTA ($I_{1110(E)}/I_{845(B)}=0.17$) > F10TC-Bi ($I_{1110(E)}/I_{845(B)}=0.02$).

These data suggest that F10TC-Bi should hydrate at the lowest rate among the analyzed cements; actually, the trend of the marker band of portlandite at about 3640 cm^{-1} confirms this interpretation. Besides the CSH hydrated silicates, this phase forms as a product of the hydration of alite and belite; as can be seen from the spectra reported in Fig. 8, the marker band of portlandite was detected in the interior of all incubated samples. In FTC-Bi, the intensity of the 3640 cm^{-1} band was higher than for wTC-Bi at any ageing time, while in F10TC-Bi this band attained the lowest intensity, in agreement with the above discussed trends that suggested the slowest hydration rate. This result is in agreement with the studies by Xu et al. [51] who have reported that the increase of the CaF_2 doping amount in tricalcium silicate paste results in a lower hydration rate. Actually, the fluorite component has been reported to play the role of a protecting film on the surface of clinker minerals, able to suppress the water penetration and movement of ions [52,53]. The formation of this phase may explain the lower hydration rate obtained for F10TC-Bi. Actually, this phase was detected on the surface of the F10TC-Bi cement upon immersion in water for 28 days (data not shown).

It must be observed that portlandite was never detected on the surface of the cements, due to its release into the DPBS medium, which underwent an increase in pH. Fig. 9 shows the trend of pH as a function of the immersion time of the cements; ageing determined a marked increase of pH since early soaking times (after 5 h pH was about 12 for all the cements). The F-doped materials exhibited the highest pH values after one day of ageing (about 13 versus 12 for the other cements). After 28 days of soaking, the DPBS media where the F-doped cements and ProRoot MTA were immersed showed a decrease of pH that still remained alkaline (about 9), while wTC-Bi maintained a pH value of about 12. In the light of these results, it appears clear that the addition of NaF had a different effect with respect to CaF_2; actually, one of the disadvantages of using CaF_2 as calcium silicate F-doping agent has been reported to be the decrease of the alkalinizing activity [50].

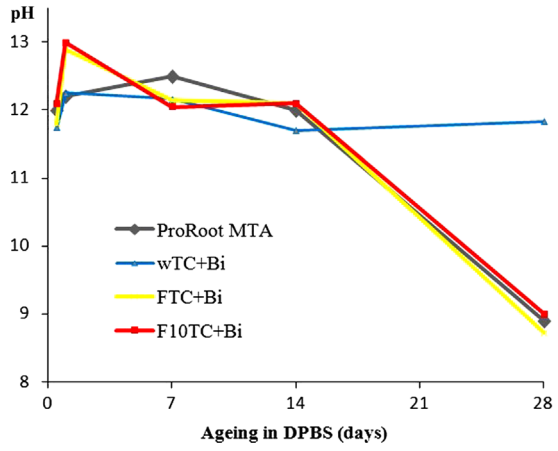

Fig. 9. pH of the DPBS medium as a function of the immersion time of the cements.

4. Conclusions

The apatite forming ability of the cements was tested upon ageing in DPBS and inspected by vibrational spectroscopy. All the tested cements showed the formation of a calcium phosphate deposit already after 5 h of soaking. Fluoride-doped cements demonstrated a higher bioactivity than the undoped wTC-Bi cement. This result was explained in relation to the nature of the deposit formed on the cements: a B-type carbonated apatite on the undoped cements and a less soluble fluoride containing B-type carbonated apatite on the fluoride-doped cements. The NaF content was found to influence the apatite forming ability; actually, the cement richer in NaF, i.e. F10TC-Bi showed a lower bioactivity than FTC-Bi, which contained only 1% w/w of NaF. This result may be explained in relation to the lower hydration rate of the former, which showed the formation of lower amounts of CSH, ettringite and portlandite phases.

References

[1] M. Torabinejad, D.J. White, US Patent Number 5,769,638; May 1995.
[2] F.R. Tay, D.H. Pashley, F.A. Rueggeberg, R.J. Loushine, R.N. Weller, Calcium phosphate phase transformation produced by the interaction of the Portland cement component of white mineral trioxide aggregate with a phosphate-containing fluid, Journal of Endodontics 33 (2007) 1347–1351.
[3] N.K. Sarkar, R. Caicado, P. Ritwik, R. Moiseyeva, I. Kawashima, Physicochemical basis of the biologic properties of mineral trioxide aggregate, Journal of Endodontics 31 (2005) 97–100.
[4] N.J. Coleman, J.W. Nicholson, K. Awosanya, A preliminary investigation of the in vitro bioactivity of white Portland cement, Cement and Concrete Research 37 (2007) 1518–1523.
[5] M.G. Gandolfi, P. Taddei, A. Tinti, E.Dorigo De Stefano, P.L. Rossi, C. Prati, Kinetics of apatite formation on a calcium-silicate cement for root-end filling during ageing in physiological-like phosphate solutions, Clinical Oral Investigations 14 (2010) 659–668.
[6] M.G. Gandolfi, K. Van Landuyt, P. Taddei, E. Modena, B. Van Meerbeek, C. Prati, ESEM-EDX Raman techniques to study ProRoot

MTA and calcium-silicate cements in wet conditions and in real-time, Journal of Endodontics 36 (2010) 851–857.
[7] M.G. Gandolfi, P. Taddei, A. Tinti, C. Prati, Apatite-forming ability of ProRoot MTA, International Journal of Endodontics 43 (2010) 917–929.
[8] P. Taddei, E. Modena, A. Tinti, F. Siboni, C. Prati, M.G. Gandolfi, Vibrational investigation on the in vitro bioactivity of commercial and experimental calcium-silicate cements for root-end endodontic therapy, Journal of Molecular Structure 993 (2011) 367–375.
[9] P. Taddei, A. Tinti, M.G. Gandolfi, P.L. Rossi, C. Prati, Ageing of calcium silicate cements for endodontic use in simulated body fluids: a micro-Raman study, Journal of Raman Spectroscopy 40 (2009) 1858–1866.
[10] D.F. Williams, Definitions in biomaterials, Proceedings of a consensus conference of the European society for biomaterials, Elsevier, New York, 1987.
[11] T. Kokubo, H. Takadama, How useful is SBF in predicting in vivo bone bioactivity?, Biomaterials 27 (2006) 2907–2915.
[12] T. Albrektsson, C. Johansson, Osteoinduction, osteoconduction and osseointegration, European Spine Journal 10 (2001) S96–S101.
[13] M.G. Gandolfi, P. Taddei, S. Siboni, E. Modena, E. Dorigo De Stefano, C. Prati, Biomimetic remineralization of human dentine using promising innovative calcium-silicate hybrid "smart" materials, Dental Materials 27 (2011) 1055–1069.
[14] M.G. Gandolfi, S. Farascioni, D.H. Pashley, G. Gasparotto, C. Prati, Calcium silicate coating derived from Portland cement as treatment for hypersensitive dentine, Journal of Dentistry 36 (2008) 565–578.
[15] M. Bohner, J. Lemaitre, Can bioactivity be tested in vitro with SBF solution?, Biomaterials 30 (2009) 2175–2179.
[16] L. Seppa, Fluoride release and effect on enamel softening by fluoride-treated and fluoride-untreated glass-ionomer specimens, Caries Research 28 (1994) 406–408.
[17] J.W. Nicholson, Adhesive dental materials, a review, International Journal of Adhesion and Adhesives 18 (1998) 229–236.
[18] K.H.W. Lau, D.J. Baylink, Molecular mechanism of action of fluoride on bone cells, Journal of Bone and Mineral Research 13 (1998) 1660–1667.
[19] O. Nakade, H. Koyama, J. Arai, H. Ariji, J. Takada, T. Kaku, Stimulation by low concentrations of fluoride of the proliferation and alkaline phosphatase activity of human dental pulp cells in vitro, Archives of Oral Biology 44 (1999) 89–92.
[20] T. Aoba, O. Fejerskov, Dental fluorosis: chemistry and biology, Critical Reviews in Oral Biology and Medicine 13 (2002) 155–170.
[21] M.G. Gandolfi, F. Iacono, K. Agee, F. Siboni, F. Tay, D.H. Pashley, C. Prati, Setting time and expansion in different soaking media of experimental accelerated calcium-silicate cements and ProRoot MTA, Oral Surgery, Oral Medicine, Oral Pathology, Oral Radiology, and Endodontics 108 (2009) E39–E45.
[22] M.G. Gandolfi, C. Prati, MTA F-doped, MTA cements used as sealers with warm gutta-percha. Long-term sealing ability study, International Endodontic Journal 43 (2010) 889–901.
[23] M.G. Gandolfi, F. Perut, G. Ciapetti, R. Mongiorgi, C. Prati, New Portland cement-based materials for endodontics mixed with articaine solution: a study of cellular response, Journal of Endodontics 34 (2008) 39–44.
[24] J. Bensted, Uses of Raman Spectroscopy in Cement Chemistry, Journal of American Ceramic Society 59 (1976) 140–143.
[25] M. Conjeaud, H. Boyer, Some possibilities of Raman microprobe in cement chemistry, Cement and Concrete Research 10 (1980) 61–70.
[26] M. Tarrida, M. Madon, B. Le Rolland, P. Colombet, An in-situ Raman-spectroscopy study of the hydration of tricalcium silicate, Advanced Cement-Based Materials 2 (1995) 15–20.
[27] L.P. Sarma, P.S.R. Prasad, N. Ravikumar, Raman spectroscopic study of phase transitions in natural gypsum, Journal of Raman Spectroscopy 29 (1998) 851–856.
[28] S. Martinez-Ramirez, S. Sanchez-Cortes, J.V. Garcia Ramos, C. Domingo, C. Fortes, M.T. Blanco-Varela, Micro-Raman spectroscopy applied to depth profiles of carbonates formed in lime mortar, Cement and Concrete Research 33 (2003) 2063–2068.
[29] T.L. Hughes, C.M. Methven, T.G.J. Jones, S.E. Pelham, P. Fletcher, C. Hall, Determining cement composition by Fourier-transform infrared-spectroscopy, Advanced Cement-Based Materials 2 (1995) 91–104.
[30] M.I. Dominguez, J. Carpena, D. Borschnek, M.A. Centeno, J.A. Odriozola, J. Rose, Apatite and Portland/apatite composite cements obtained using a hydrothermal method for retaining heavy metals, Journal of Hazardous Materials 150 (2008) 99–108.
[31] M.Y.A. Mollah, W. Yu, R. Schennach, D.L. Cocke, A Fourier transform infrared spectroscopic investigation of the early hydration of Portland cement and the influence of sodium lignosulfonate, Cement and Concrete Research 30 (2000) 267–273.
[32] F.A. Andersen, L. Brecevic, Infrared spectra of amorphous and crystalline calcium-carbonate, Acta Chemica Scandinavica 45 (1991) 1018–1024.
[33] F.Z. Zakaria, J. Mihaly, I. Sajo, R. Katona, L. Haiba, F.A. Aziz, J. Mink, FT-Raman and FTIR spectroscopic characterization of biogenic carbonates from Philippine venus seashell and porites sp coral, Journal of Raman Spectroscopy 39 (2008) 1204–1209.
[34] H.W. Van der Marel, H. Beutelspacher, Atlas of Infrared Spectroscopy of Clay Minerals and Their Admixtures, Elsevier, Amsterdam, 1976.
[35] D.G.A. Nelson, J.D.B. Featherstone, Preparation, analysis, and characterization of carbonated apatites, Calcified Tissue International 34 (1982) S69–S81.
[36] M.G. Gandolfi, P. Taddei, F. Siboni, E. Modena, G. Ciapetti, C. Prati, Development of the foremost light-curable calcium-silicate MTA cement as root-end in oral surgery Chemical–physical properties, bioactivity and biological behavior, Dental Materials 27 (2011) e134–e157.
[37] C.S. Deng, C. Breen, J. Yarwood, S. Habesch, J. Phipps, B. Craster, G. Maitland, Ageing of oilfield cement at high humidity: a combined FEG-ESEM and Raman microscopic investigation, Journal of Materials Chemistry 12 (2002) 3105–3112.
[38] R.M. Wilson, J.C. Elliott, S.E.P. Dowker, L.M. Rodriguez-Lorenzo, Rietveld structure refinement of precipitated carbonate apatite using neutron diffraction data, Biomaterials 25 (2004) 2205–2213.
[39] J.D.B. Featherstone, S. Pearson, R.Z. LeGeros, An IR method for quantification of carbonate in carbonated-apatites, Caries Research 18 (1984) 63–66.
[40] V.M. Bhatnagar, Infrared spectra of hydroxyapatite and fluorapatite, Bulletin de la Société Chimique de France 8 (1968) 1771–1773.
[41] C.H. Amberg, H.C. Luk, K.P. Wagstaff, The fluoridation of nonstoichiometric calcium hydroxyapatite. An infrared study, Canadian Journal of Chemistry 52 (1974) 4001–4006.
[42] F. Freund, R.M. Knobel, Distribution of fluorine in hydroxyapatite studied by infrared spectroscopy, Journal of the Chemical Society, Dalton Transactions (1977) 1136–1140.
[43] I. Nikčević, V. Jokanović, M. Mitrić, Z. Nedić, D. Makovec, D. Uskoković, Mechanochemical synthesis of nanostructured fluorapatite/fluorhydroxyapatite and carbonated fluorapatite/fluorhydroxyapatite, Journal of Solid State Chemistry 177 (2004) 2565–2574.
[44] K. Sundarsanan, R.A. Young, Significant precision in crystal structure details: Holly Springs hydoxyapatite, Acta Crystallographica B 25 (1969) 1534–1543.
[45] R.Y. Whitehead, L.C. Lucas, W.R. Lacefield, The effect of dissolution on plasma sprayed hydroxylapatite coatings on titanium, Clinical Materials 12 (1993) 31–39.
[46] L.M. Silverstone, The effect of fluoride in the remineralization of enamel caries and caries-like lesions in vitro, Journal of Public Health Dentistry 42 (1982) 42–53.
[47] L. Savarino, S. Stea, G. Ciapetti, D. Granchi, M.E. Donati, M. Cervellati, M. Visentin, A. Moroni, A. Pizzoferrato, The interface of bone microstructure and an innovative coating: an X-ray diffraction study, Journal of Biomedical Materials Research 40 (1998) 86–91.
[48] L. Gineste, M. Gineste, X. Ranz, A. Ellefterion, A. Guilhem, N. Rouquet, P. Frayssinet, Degradation of hydroxylapatite, fluorapatite, and fluorhydroxyapatite coatings of dental implants in dogs, Journal of Biomedical Materials Research 48 (1999) 224–234.
[49] R.Z. LeGeros, J.P. LeGeros, Dense hydroxyapatite, in: L.L. Hench, J. Wilson (Eds.), An Introduction to Bioceramics, Advances in Applied Ceramics, 1, World Scientific Publishing Co., London, 1998, pp. 139–180.

[50] Q. Lin, Y. Li, X. Lan, C. Lu, Y. Chen, Z. Xu, The apatite formation ability of CaF_2 doping tricalcium silicates in simulated body fluid, Biomedical Materials 4 (2009) 045005.

[51] Z. Xu, Q. Lin, Y. Li, X. Lan, C. Lu, An evaluation of CaF_2 doping tricalcium silicate as dental restorative materials, Advance Materials Research 47–50 (2008) 1339–1342.

[52] H.F.W. Taylar, The Cement Chemistry, Academic Press Limited, London, 1990, pp. 386.

[53] S. Chandra (Ed.), Waste Materials Used in Concrete Manufacturing, William Andrew Inc., Norwich, N.Y., 1996.